https://doi.org/10.5194/egusphere-2023-918
Preprint. Discussion started: 8 May 2023

Intraseasonal and interannual variability of sea temperature in the Arabian Sea Warm Pool

Na Li[1], Xueming Zhu[1], Hui Wang[2, 3], Shouwen Zhang[1, *], Xidong Wang[1, 4]

[1]School of marine sciences, Sun Yat-sen University &Southern Marine Science and Engineering Guangdong Laboratory (Zhuhai), Zhuhai, China
[2]Key Laboratory of Research on Marine Hazards Forecasting, National Marine Environmental Forecasting Center, Beijing, China
[3]Institute of Marine Science and Technology, Shandong University, Qingdao, China
[4]Key Laboratory of Marine Hazards Forecasting, Ministry of Natural Resources, Hohai University, Nanjing, China.

Correspondence to: Shouwen Zhang (zhangshouwen@sml-zhuhai.cn)

Abstract. The Arabian Sea Warm Pool (ASWP) is a part of the Indian Ocean Warm Pool, formed in the Arabian Sea before the onset of the Indian Ocean summer monsoon. The ASWP has a significant impact on climate change in the Indian Peninsula and globally. In this study, we examined the Intraseasonal and interannual variability of sea temperature in the Arabian Sea Warm Pool using the latest 5-day SODA reanalysis dataset. We quantified the contributions of sea surface heat flux, advection, and vertical entrainment to the sea surface temperature using mixed-layer heat budget analysis. We also used a lead lag correlation method to examine the relationship between the interannual variability of the ASWP and various large-scale modes in the Indo-Pacific Ocean. We found that the ASWP formed in April and decayed in June. Its formation and decay processes were asymmetrical, with the decay rate being twice as fast as the formation rate. During the ASWP development phase, the sea surface heat flux had the largest impact on the mixed layer temperature with a contribution of up to 85%. Its impact was divided into the net heat flux at the sea surface (0.41–0.50°C/5 day) and the short-wave radiation loss penetrating the mixed layer (from –0.08°C/5 day to –0.17°C/5 day). During the decay phase, the cooling effect of the vertical entrainment (from –0.05°C/5 day to –0.18°C/5 day) on the temperature variation increased and dominated the temperature variation jointly with the sea surface heat flux. We also found that the ASWP has strong interannual variability related to the consistent warming of the Indian Ocean basin. The lead lag correlation indicated that ASWP had a good synchronous correlation with the Indian Ocean Dipole. ASWP had the largest correlation coefficient at a lag of 5–7 months of niño3.4 index, showing the characteristics of modulation by ENSO. The ASWP was more significant (insignificant) in the following year before the summer monsoon after an El Niño (La Niña) event that peaked in the previous winter.

1 Introduction

Tropical warm pools greatly affect atmospheric systems and oscillation modes, such as the monsoon, cyclones, El Niño and La Niña, and the Indian Ocean Dipole (IOD) (Lau and Chan, 1988; Webster and Lukas, 1992). Therefore, the study of warm pools and their climate effects is important for the understanding of global climate change. The Arabian Sea warm pool

https://doi.org/10.5194/egusphere-2023-918
Preprint. Discussion started: 8 May 2023

(ASWP) is part of the Indian Ocean warm pool (IOWP). It forms in the Arabian Sea before the onset of the Indian Ocean summer monsoon. Its sea surface temperature reaches its maximum before the summer monsoon onset and gradually dissipates with the onset of the monsoon. It has a considerable influence on the monsoon onset eddies and other sea–air interactions, representing a remarkable mechanism for the regulation of the regional climate system. A deeper exploration of the regulating factors of the evolution of the ASWP and its relationship with the large-scale modes can not only enhance the scientific knowledge of the changes of the ASWP but also provide a theoretical basis for the prediction and forecasting of the ASWP.

In addition to being a component of the IOWP, the ASWP also demonstrates evolutionary traits that are distinct from those of the IOWP. Many studies have reported that high SST in the southeastern Arabian Sea (AS) occurs only before the onset of the summer monsoon. In the MONEX-79 monsoon experiment, Seetharamayya and Master(1984) noted a warm pool (SST > 30.5°C) in the southeastern AS one week before the summer monsoon outbreak. Krishnamurt et al. (1988) noted an extreme value in the northern Indian Ocean before and after the monsoon outbreak in 1979. Joseph (1990) also suggested that SST maxima occurred one week before the summer monsoon outbreak in the southeastern AS during 1961–1972.

Rao and Sivakumar (1999) used monthly climatology observation and model simulations to examine plausible mechanisms for the gradual build-up of ASWP. They found that the heat balance of the mixed layer essentially reflected the distribution of the net heat flux, while advection processes played a modulating role. Debasis Sengupta's (2008) experiments in two different phases during Arabian Sea Monsoon Experiment determined that in the warming phase, the temperature rose mainly because of heat absorbed within the mixed layer. In the second phase, the penetrative fluxes of solar radiation and advective cooling were together responsible for the rapid SST cooling. Kumar (2009) used a three-dimensional circulation model to study the growth and decay characteristics of ASWP in May 2000. He found that when the heat flux was not considered, the AS temperature continued to cool and no warm pools appeared. When salinity changes were not considered, the ASWP still existed, but the horizontal extent of the warm pools decreased and the warming rate became slower. Sanilkumar et al. (2004) demonstrated that the vertical extent and stratification of low salinity waters affected the intensity of heating and thickness of the warm pool, while the extent of low salinity waters regulated the warm pool's horizontal coverage. However, Kurian and Vinayachandran (2007) cast doubt on this theory and proposed an alternative explanation for the warming that occurred in the early phases of the warm pool. They found that the Western Ghats' orographic impact decreased wind speed in the Arabian Sea's southeast and, consequently, latent heat loss, resulting in a positive heat flux into the ocean.

Using in-situ observations and satellite data, Sabu and Revichandran (2011) examined the relative importance and contribution of various processes to the total heat budget of the mixed layer of the ASWP (29.5°C) during the spring intermonsoon (March–April 2004). They discovered that advection had a role in transporting the warm water from the coastal region to the far west, while surface heat flux was the primary factor in the mixed layer warming in the northern part of the warm pool. In the southern part of the warm pool, the eddy-induced horizontal mixing provided a substantial amount of heat spreading, which influenced the mixed layer temperature evolution. Shankar et al. (1997) then suggested that the

https://doi.org/10.5194/egusphere-2023-918
Preprint. Discussion started: 8 May 2023

formation of the ASWP was related to the Kelvin wave and its radiated Rossby wave in Peninsular India and that the fluctuations led to the formation of the Laccadive High over the AS, thus producing the ASWP.

There is some interannual variation in the ASWP, which may be linked to the variation of large-scale modes such as the Indian Ocean Basin (IOB), IOD, and the El Niño-Southern Oscillation (ENSO). According to Lau (2000) and Chowdary et al. (2007), zonal movement of the convergence centers linked to the Walker circulation is the main mechanism by which ENSO effects are transmitted to the Tropical Indian Ocean (TIO). This led to subsidence in the eastern TIO, which reduced rainfall and caused abnormal easterly winds. Thereafter, the TIO as a whole warmed as a result of an increase in short-wave radiation and a drop in the latent heat flux. This warming was the dominant mode of interannual variability in TIO temperature. When an El Niño event develops, the size of the Indo-Pacific warm pool increases as it extends eastward in the Pacific sector and westward in the Indian Ocean sector, and vice versa for a La Niña. The response of the warm pool intensity to ENSO does not reach its peak until about 5 months after ENSO peaks. The displacement and intensity changes in the Indo-Pacific warm pool affect the onset, intensity, and period of ENSO (Picaut et al., 1996).

Webster (1999) and Saji et al. (1999) demonstrated that sea-air coupling processes allow the TIO to create its internal modes of SST variability, i.e., the Indian Ocean dipole. It is worth noting that in recent years, roughly half of the IOD coincided with El Niño, while the other events were caused by internal TIO development (Meyers et al., 2007). ENSO variability was discovered to have an impact on the periodicity, strength, and formation processes of the IOD during the years of co-occurrence (Annamalai et al., 2003; Behera et al., 2006). IOD was more significant and persistent during the years of co-occurrence, and it was characterized by both eastern cooling and western warming. For the majority of fluctuations in the 10°N–10°S area, the observed interannual variability in ocean mixed layer depth—a crucial component that affects the SST variability—was related to the IOD. In the equatorial and southeast Indian Oceans, a shallow mixed layer was linked with the IOD-positive phases, while the south-central Indian Ocean saw a deepening (Rao et al., 2015; Thompson et al., 2006).

Even though some researchers have analyzed the climatological features of ASWP, their work has mostly been limited to monthly averages of key features. The ASWP evolutionary features and their related processes were not well-examined due to low data resolution and high variability within that data. However, a variety of marine data with high spatial and temporal resolution and good quality now provides the possibility for deeper research. Although the effects of ENSO, IOD, and the Indo-Pacific warm pool have been studied, few scientists have explored the relationship between various large-scale modes and smaller-scale seas, such as the Arabian Sea. Based on the results of previous studies, this paper defines the threshold of the ASWP as 30°C. Using high-resolution satellite remote sensing and reanalysis data, we investigated the intraseasonal and interannual variability of the ASWP, investigated the causes of the intraseasonal variability of the ASWP using heat balance analysis, and investigated the interannual variability of the ASWP and its relationship with IOD and ENSO using lead lag correlations.

The overall framework of this paper is as follows: Section 2 briefly introduces the data sources used in this paper and the research methods adopted; Section 3 explains the intraseasonal characteristics of the ASWP and analyzes its thermodynamic diagnosis using the mixed layer diagnostic formula; Section 4 analyzes the interannual variability characteristics of the

https://doi.org/10.5194/egusphere-2023-918
Preprint. Discussion started: 8 May 2023

ASWP with IOB, IOD, and ENSO; and Section 5 summarizes the main research results and provides an outlook for future work.

2 Data and Methods

2.1 SODA Ocean Dataset

The SODA3.7.2 ocean dataset is derived from the Simple Ocean Data Assimilation (SODA), which contains various parameters such as temperature, density, salinity, sea surface height, and current velocity, with a resolution of 0.25°×0.25° in the latitudinal and longitudinal directions and 50 layers in the vertical direction, up to 5400 m. The time period of the data is from 1980 to 2020, with a time interval of 5 days (Giese, 2005).

2.2 JRA-55

JRA-55, the forcing field used in SODA 3.7.2, is the Japanese second global atmospheric reanalysis project, originating from the Japan Meteorological Agency. Compared with its predecessor, JRA-25, JRA-55 is based on a new data assimilation and prediction system (DA) that improves upon many deficiencies found in the first Japanese reanalysis. These improvements have come about by implementing a higher spatial resolution (TL319L60), a new radiation scheme, four-dimensional variational data assimilation (4D-Var) with variational bias correction (VarBC) for satellite radiances, and the introduction of greenhouse gases with time-varying concentrations. The data time period is from 1958 to the present. This paper uses day-by-day sea–air heat flux data, including long-wave radiation, short-wave radiation, sensible heat, and latent heat.

2.3 Methods

To investigate the specific processes affecting the SST variation, this paper uses the SODA and JRA-55 datasets for the mixed layer thermodynamic diagnostic analysis in the ASWP (SST>30°C). The changes in mixed layer temperature with time were dominated by sea surface heat flux forcing (SHF), horizontal advection (ADV), and vertical entrainment (ENT). To perform a quantitative and specific analysis of each, we used equations (2.1)–(2.4) (Li et al., 2016) for mixed layer diagnosis.

$$\frac{\partial T}{\partial t} = SHF + ADV + ENT + R \tag{2.1}$$

$$SHF = Q_{net} - Q_{loss} = \frac{Q_{sw} - Q_{lw} \pm Q_{sh} \pm Q_{lh}}{\rho_0 c h} - \frac{Q_{sw}[re^{-\frac{h}{\beta_R}} + (1-r)e^{-\frac{h}{\beta_B}}]}{\rho_0 c h} \tag{2.2}$$

$$ADV = -U\frac{\partial T}{\partial x} - V\frac{\partial T}{\partial y} \tag{2.3}$$

$$ENT = -(W_h + H\frac{\partial h}{\partial t} + U\frac{\partial h}{\partial x} + V\frac{\partial h}{\partial y})\frac{T - T_h}{h} \tag{2.4}$$

$$ENT1 = -W_h\frac{T - T_h}{h} \tag{2.4.a}$$

https://doi.org/10.5194/egusphere-2023-918
Preprint. Discussion started: 8 May 2023

$$ENT2 = -H\frac{\partial h}{\partial t}\frac{T-T_h}{h} \quad (2.4.b)$$

$$ENT3 = -(U\frac{\partial h}{\partial x} + V\frac{\partial h}{\partial y})\frac{T-T_h}{h} \quad (2.4.c)$$

The left side of Eq. (2.1) represents the local variation term of mixed layer temperature with time. The SHF, ADV, ENT, and R represent the surface heat flux, horizontal advection, vertical entrainment, and residual term, respectively. T represents the average mixed layer temperature; $\frac{\partial T}{\partial x}$ and $\frac{\partial T}{\partial y}$ represent the latitudinal and longitudinal spatial variation of mixed layer temperature, respectively. Q_{net} represents the surface net heat flux, and its value is the sum of short-wave radiation flux Q_{sw}, long-wave radiation flux Q_{lw}, sensible heat Q_{sh}, and latent heat Q_{lh}. r=0.62 is the red light fraction, β_R=0.6 m is the penetration depth scale of red light, and β_B=10 m is the penetration depth scale of blue light. h is the depth of the mixed layer. In this paper, the mixed layer depth has been defined as the depth at which the seawater is 0.03 kg/m3 higher than the surface density. U, V is the average horizontal current velocity of the mixed layer. W_h is the bottom of the mixed layer. T_h is the temperature at the bottom 10 m of the mixed layer; H is a dimensionless number that equals 0 when $\frac{\partial h}{\partial t} \leq 0$ and 1 when $\frac{\partial h}{\partial t} > 0$. ENT1, ENT2, and ENT3 in equations (2.4.a)–(2.4.c) denote the entrainment due to the vertical velocity, the tendency of the mixed layer depth, and the "advection of the mixed layer depth," respectively. The term R is the residual term, representing unresolved processes such as the horizontal and vertical diffusion and errors in the estimation of terms.

This study also used empirical orthogonal function (EOF) analysis to separate the spatial and temporal characteristics of the ASWP and study the relationship between the ASWP and IOD/ENSO using lead lag correlation.

https://doi.org/10.5194/egusphere-2023-918
Preprint. Discussion started: 8 May 2023

3 Intraseasonal variability of the ASWP

3.1 Intraseasonal variation characteristics of the ASWP

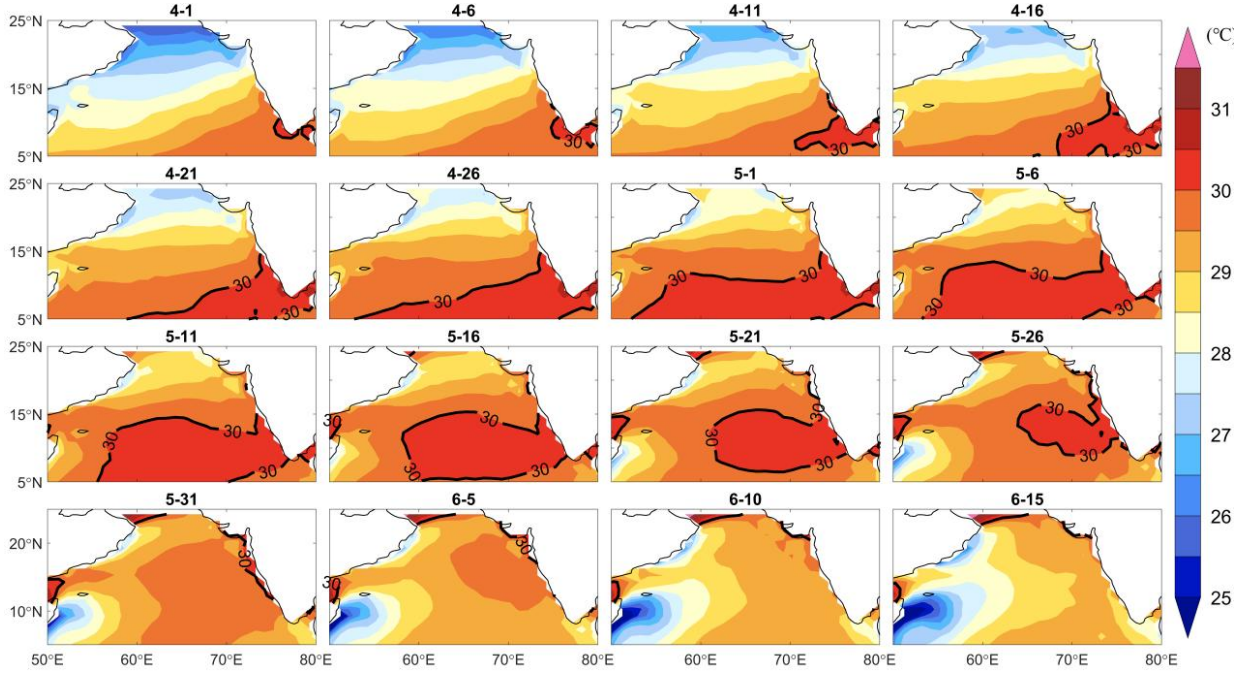

Figure 1: Climatological mean SST (1980–2016) in April–June, where the black contour is the 30°C contour.

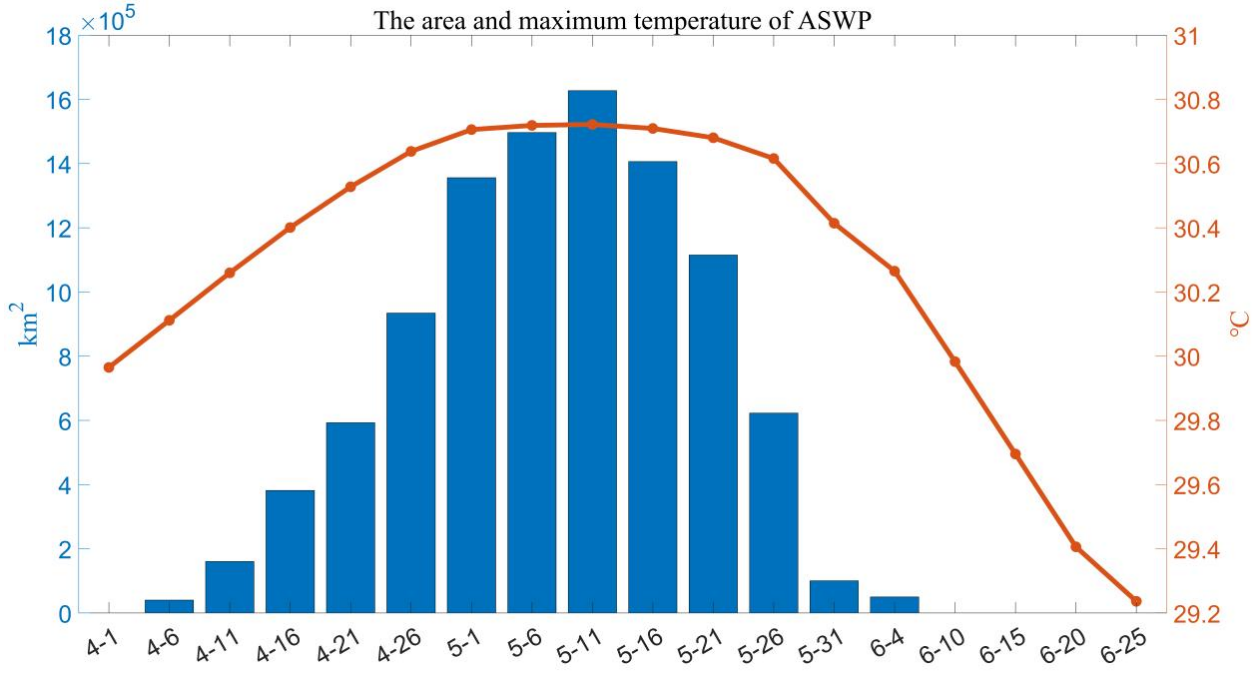

https://doi.org/10.5194/egusphere-2023-918
Preprint. Discussion started: 8 May 2023

Figure 2: Climatological time series of the area and maximum temperature of ASWP, where the blue bars represent the warm pool area (km^2) and the red dashes represent the maximum warm pool temperature (°C).

The entire formation and extinction of the ASWP is generally completed in April, May, and June. Therefore, using the SODA climatological mean sea surface temperature from April to June 1980–2016, its area and maximum temperature were calculated to obtain Figures 1 and 2. It can be seen that, on average, the sea surface temperature at the southern tip of the Indian Peninsula began to exceed 30°C on April 1, after which the high-temperature area continued to extend westward and northward. After that, the warm pools expanded to their maximum extent ($1.63*10^6$ km^2) on May 11, when the warm pools were in a strong stage. Thereafter, the warm pools decayed rapidly and disappeared almost completely in early June. It is obvious from Figure 2 that the formation and decay of the warm pool are not symmetrical, as it takes about 1.5 months (6 weeks) from the beginning of the warm pool to its peak, while the warm pool takes only 3 weeks from the beginning of decay to its complete disappearance. The decay rate is twice as fast as the development rate. The mechanism influencing this asymmetry in formation and decay is discussed below.

3.2 ASWP mixed layer heat budget analysis

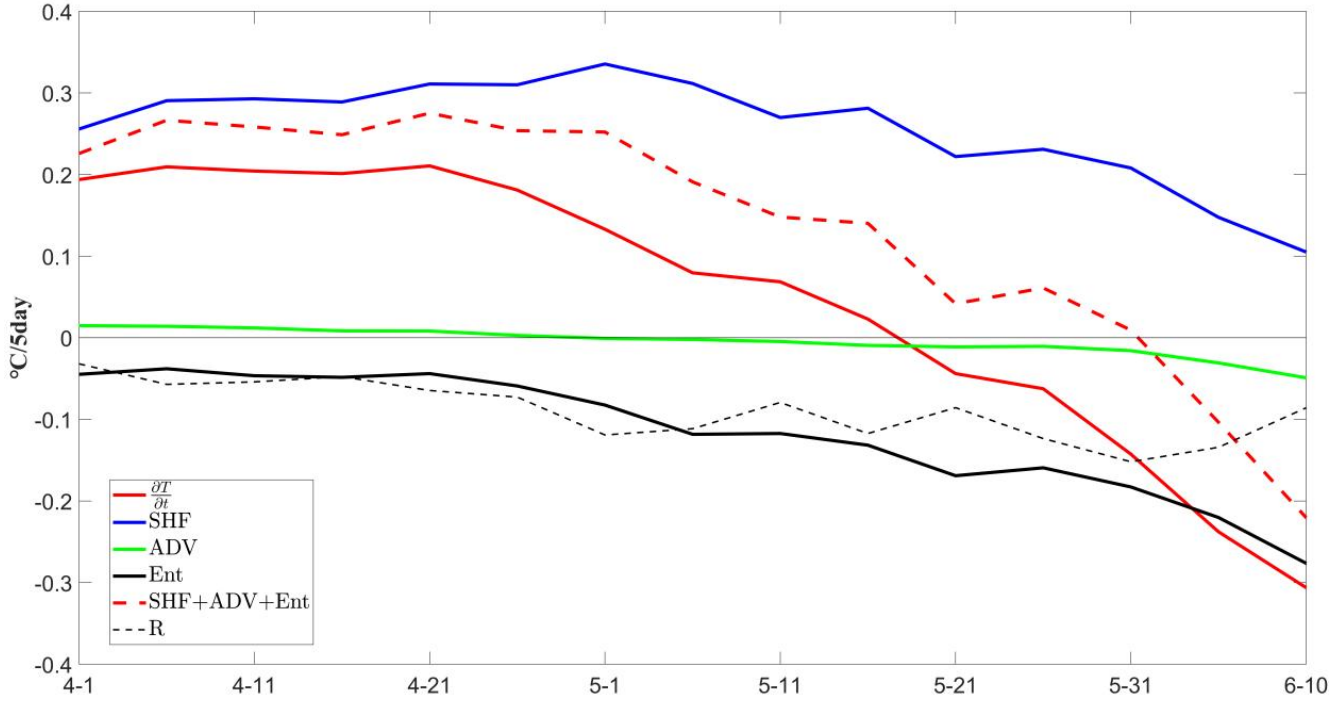

Figure 3: Contribution of different processes to the temperature variation of the warm pool mixed layer in the Arabian Sea (°C/5 day), where $\frac{\partial T}{\partial t}$ is the temperature variation of the warm pool mixed layer with time, SHF represents the surface heat flux, ADV represents the horizontal advection, ENT represents the vertical entrainment, and R represents the residual term.

https://doi.org/10.5194/egusphere-2023-918
Preprint. Discussion started: 8 May 2023

To investigate the influence and contribution of different factors during the warm pool evolution, a mixed layer heat budget analysis was performed using SODA 3.7.2 reanalysis data and JRA-55 heat flux data. The results are shown in Figure 3. Throughout the evolution of ASWP, the sums of SHF, ADV, and ENT were basically consistent with the trend of mixed layer temperature. The residual term R was also maintained within 0.1°C/5 day, indicating that the heat balance equation was closed and the variation of ASWP SST was mainly related to these three terms. Therefore, these three terms can be used to explore the evolutionary mechanism of ASWP qualitatively and quantitatively.

The variation in ASWP mixed layer temperature was asymmetric. From April 1 to May 16, $\frac{\partial T}{\partial t}$ was greater than zero, and the mixed layer SST gradually increased as ASWP developed. After May 21, $\frac{\partial T}{\partial t}$ was less than zero, and the mixed layer SST rapidly decreased, corresponding to the rapid decay of the warm pool. SHF consistently dominated the warm pool throughout the warming phase, with an influence of up to 0.34°C/5 day. The overall trend of SST was consistent with SHF. ADV and ENT had less influence on the SST variation, and the ENT played a weak cooling role. In the cooling phase, the SHF gradually decreased and the ENT strengthened, up to −0.27°C/5 day. The effect of ADV was always small, not more than 0.1°C/5 day. The following is a specific and detailed analysis of the mechanism and effect of each process.

3.2.1 Surface heat flux

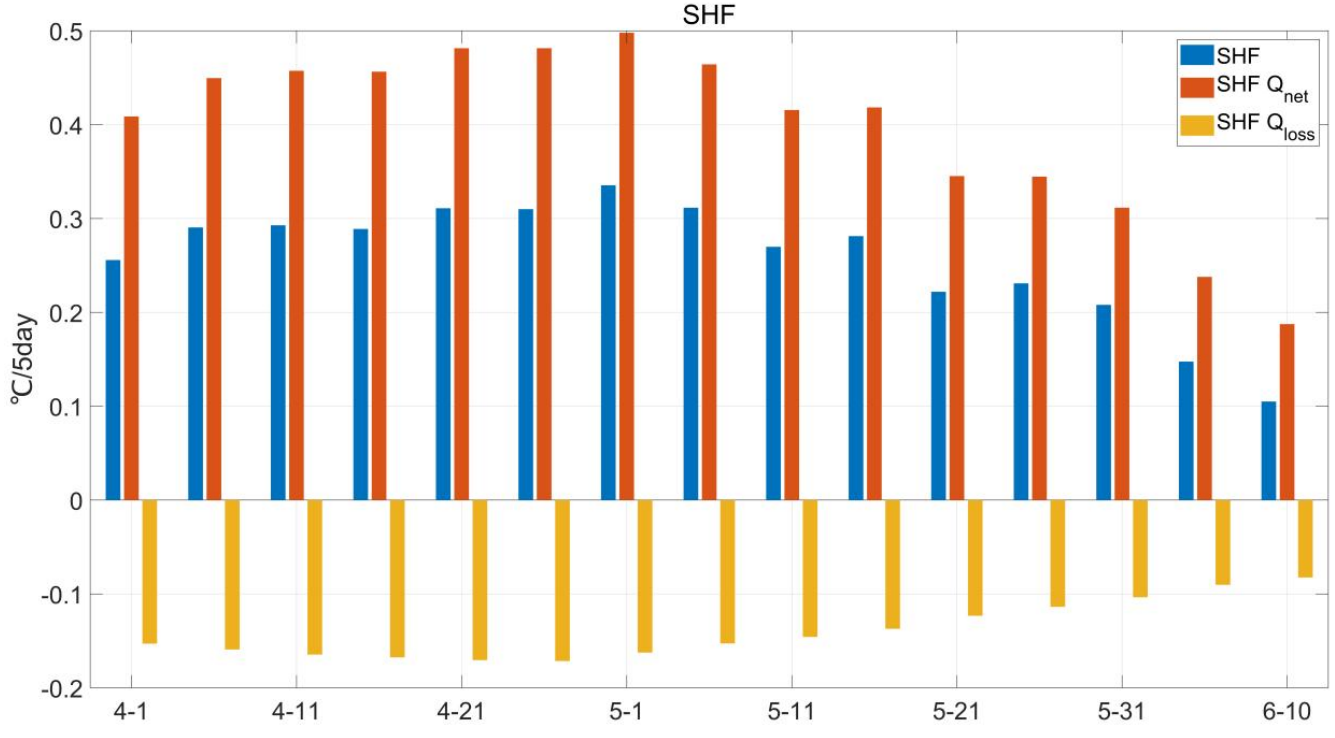

https://doi.org/10.5194/egusphere-2023-918
Preprint. Discussion started: 8 May 2023

Figure 4: Contribution of the surface heat flux to the warm pool mixed layer temperature (°C/5 day), where blue represents the total surface heat flux, red represents the contribution of the net sea air heat flux, and yellow represents the contribution of the shortwave radiation loss penetrating the mixed layer.

The contribution of SHF to $\frac{\partial T}{\partial t}$ ranged from 0.11°C/5 day to 0.34°C/5 day (Figure 4), always playing a heating role. From April to early May, the contribution of SHF to temperature was around 0.3°C/5 day, indicating that SHF provided substantial thermal support for the mixed layer temperature increase. By early June, the contribution of SHF to temperature dropped below 0.2°C/5 day, indicating that the thermal support provided by SHF to the mixed layer temperature decreased. The effect of SHF on warm pool temperature can be divided into two parts that are caused by sea–air interaction ($SHF_{Q_{net}}$) and the loss of short-wave radiation penetrating the mixed layer ($SHF_{Q_{loss}}$). The contribution of $SHF_{Q_{net}}$ gradually increased from 0.41°C/5 day to 0.50°C/5 day in April. It increased slowly but remained at a relatively high level, indicating that the continuous heating of the mixed layer by the sea air heat flux was the main source of heat that caused the rapid warming of the mixed layer. Then it gradually decreased over a long period of time to a very low level. After mid-June, the contribution of $SHF_{Q_{net}}$ decreased to below 0.2°C/5 day, which indicated that the weakening of the intensity of the heating of the mixed layer by the sea air heat flux is an important reason for the decrease of the mixed layer temperature. Similar to $SHF_{Q_{net}}$, $SHF_{Q_{loss}}$ also gradually increased to –0.17°C/5 day in April and then decreased. From April to June, $SHF_{Q_{net}}$ was always greater than $SHF_{Q_{loss}}$, making the SHF always positive. In other words, the mixed layer always received heat from the atmosphere.

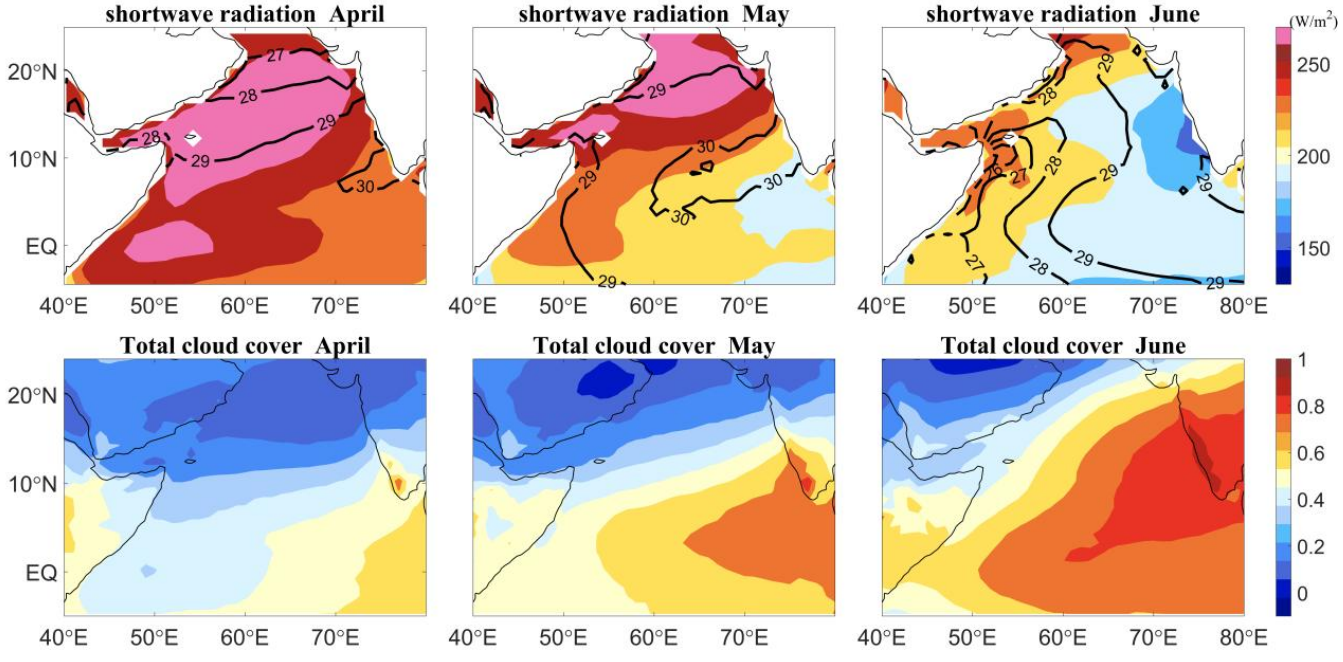

Figure 5: The upper panel: Monthly climatology of shortwave radiation flux (color shading; W/m²) and mixed layer temperature (black contours; °C). The lower panel: the distribution of total cloud coverage.

https://doi.org/10.5194/egusphere-2023-918
Preprint. Discussion started: 8 May 2023

$SHF_{Q_{net}}$ is related to sensible heat, latent heat, longwave radiation flux, and shortwave radiation flux (SWR). SWR was the largest contributor (190–283 W/m^2) and was always positive, indicating that the main source of heat in the warm pool was shortwave radiation from the sun. Therefore, we focused on the variation in SWR in the Arabian Sea in combination with cloud coverage (Figure 5). In April, the clear sky and lack of clouds over the Arabian Sea mean the sea surface can receive more SWR than at other times. The SWR was above 240 W/m^2 throughout the Arabian Sea, with a clear high value in the center of the Arabian Sea. In May, when the shortwave radiation flux had decreased (230 W/m^2), the temperature of the warm pool reached its highest. When the summer monsoon broke out, the atmospheric convective activity was strong and the cloud coverage over the sea was high, leading to a decrease in the shortwave radiation entering the mixed layer. The shortwave radiation dropped to below 220 W/m^2, with a clear low value center (<180 W/m^2) in the southeast of the Arabian Sea. In addition, although the variation of SST was roughly in line with the trend of SWR, the variation of SST had a lag time of about one month compared with SWR. This trend occurred because seawater has a large specific heat capacity and there is a certain lag in the variation of SST.

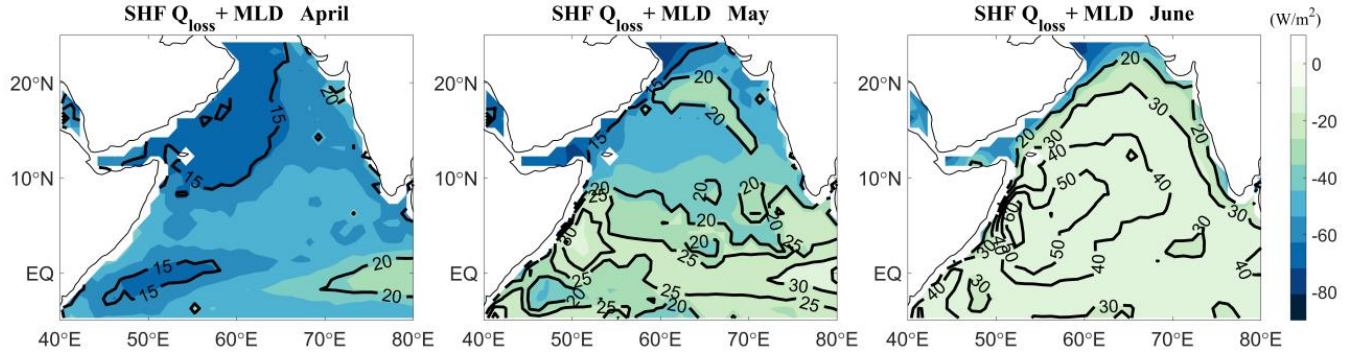

Figure 6: Monthly climatology of shortwave radiation loss penetrating the mixed layer (color shading; W/m^2) and the depth of the mixed layer (black contours; m).

$SHF_{Q_{loss}}$ was related to the mixed layer depth and was negatively correlated with it (Figure 6). In April, the wind speed over the Arabian Sea was low, making the mixed layer depth shallow (<15 m). Shortwave radiation can penetrate the mixed layer at this time (−55 W/m^2) and heat the subsurface seawater. In May, when the summer monsoon was about to break out, increased wind speed strengthened the mixing, leading to a deeper mixed layer (25 m) and a decrease in the shortwave radiation penetrating the mixed layer (−37 W/m^2). In June, when the summer monsoon was fully formed, the mixing layer became deeper (>30 m) throughout the Arabian Sea, which greatly inhibited the penetration of shortwave radiation flux into the mixed layer (−9 W/m^2).

https://doi.org/10.5194/egusphere-2023-918
Preprint. Discussion started: 8 May 2023

3.2.2 Vertical entrainment

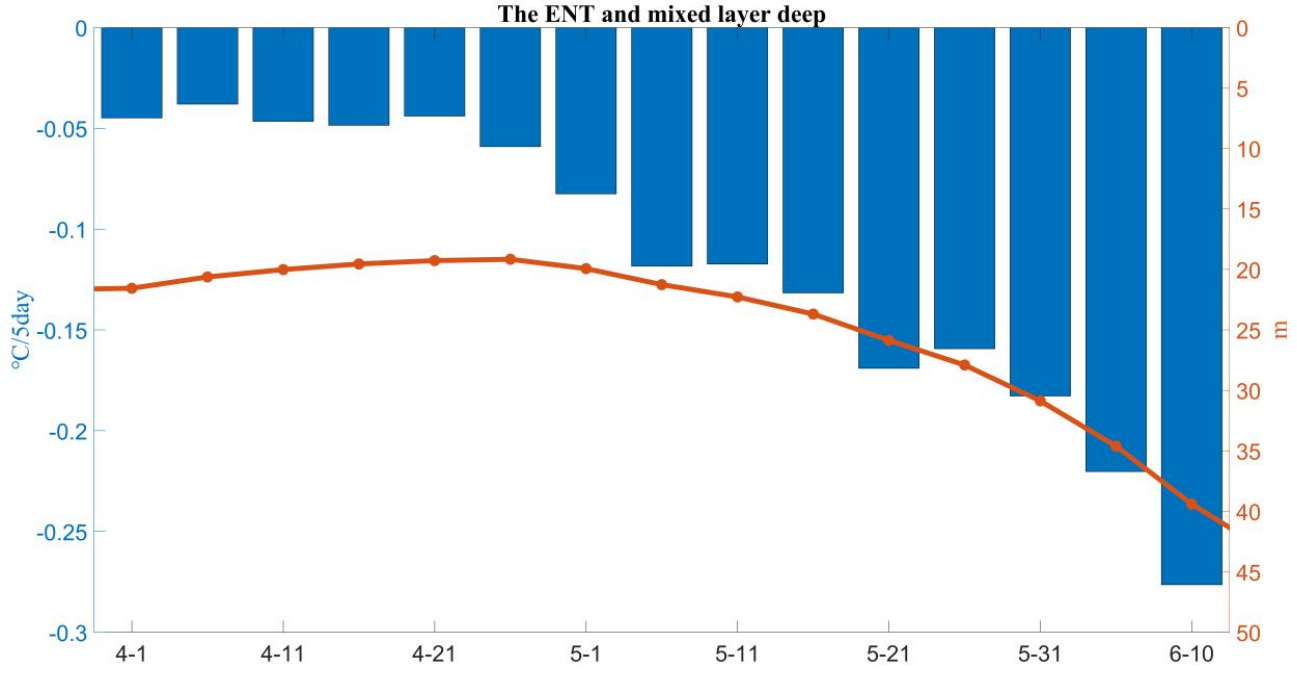

Figure 7: Variation of the vertical entrainment and mixed layer depth, where the blue bar represents the vertical entrainment (°C/5 day) and the red line represents the mixed layer depth (m).

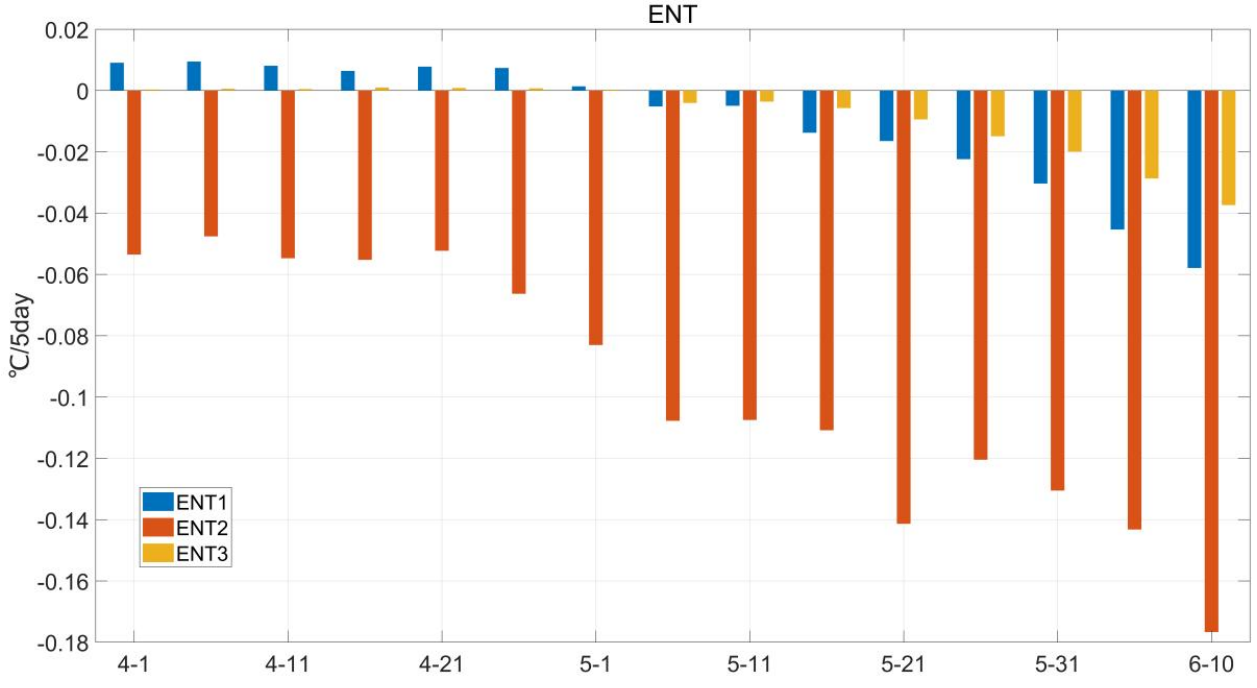

Figure 8: Contribution of each term in the vertical entrainment to the temperature change in the warm pool mixed layer.

https://doi.org/10.5194/egusphere-2023-918
Preprint. Discussion started: 8 May 2023

The contribution of ENT to temperature ranged from –0.04°C/5 day to –0.28°C/5 day (Figure 7), always acting as a cooling effect and intensifying over time. Together with the gradual decrease in SHF, it led to a rapid cooling of the ASWP. During the development phase of the warm pool, the cooling effect of ENT was weak, accounting for only 16%–20%. After May 1, the cooling effect intensified up to 58%. The effect of ENT on SST can be divided into three parts: the entrainment due to the vertical velocity (ENT1), the entrainment due to the tendency of the mixed layer depth (ENT2), and the entrainment due to "advection of the mixed layer depth" (ENT3). The cooling effect due to the local variation of the mixed layer was the strongest and almost dominated, ranging from –0.05°C/5 day to –0.18°C/5 day (Figure 8).

The vertical entrainment is related to vertical velocity, temperature difference, mixed layer depth, and its variation. In the development stage of the ASWP, the low wind speed made the mixed layer shallower and thus more sensitive to heat flux. The shallow mixed layer made the upper seawater temperature rise rapidly, while the seawater below the mixed layer warmed more slowly, increasing the vertical temperature gradient at the bottom of the mixed layer. When the change in the mixed layer depth was small, the cooling effect of entrainment was weak, and the ASWP was maintained. When the mixing of the upper seawater in terms of temperature and salinity is inconsistent, the thermocline and mixed layer will differ, and a barrier layer will be formed between the bottom of the mixed layer and the top of the thermocline (Sprintall and Tomczak, 1992). The barrier layer has the characteristics of a strong salinity gradient and high gravitational stability, which makes it difficult to transport heat from top to bottom by mixing. A strong and stable salinity stratification can effectively inhibit the transfer of non-solar radiation flux to the interior of the ocean, which leads to the warming of the upper mixed layer. However, the existence of the barrier layer can inhibit the cold water of the thermocline into the mixed layer, which is not conducive to the exchange of heat, momentum, mass, and nutrients between the mixed layer and the thermocline (Pang Shanshan, 2021). For this reason, the low saline water brought from the Bay of Bengal contributed to the formation of the barrier layer and sustained the ASWP by effectively suppressing the vertical mixing of the upper ocean and causing a warming of the upper mixed layer in the local ocean. In the late stage of ASWP evolution, with the imminent outbreak of the summer monsoon, the stirring effect of wind started to increase, the upper layer junction was disrupted, and the cooling effect of entrainment was enhanced, which accelerated the decay of the ASWP (Liu Yanliang, 2013).

Vertical entrainment is associated with wind stress vorticity and Rossby waves. On the one hand, Positive (negative) surface-wind-stress curl shoals (deepens) the pycnocline in the northern hemisphere via Ekman divergence (convergence) in the near-surface layer, which is helpful (unhelpful) to the formation of warm pools (Bauer, 1991). On the other hand, the pycnocline topography of this area appears to be modulated by a mode-2 Rossby wave that propagates from off south-west India into the interior of the AS from February to June, according to several model solutions (Bruce et al., 1994). Between January and May, a positive surface-wind-stress curl and a south-westward-propagating mode-2 Rossby wave from off south-west India caused a shoaling of the pycnocline by around 20 m (Rao and Sivakumar, 1999).

https://doi.org/10.5194/egusphere-2023-918
Preprint. Discussion started: 8 May 2023

3.2.3 Horizontal advection

The contribution of ADV to $\frac{\partial T}{\partial t}$ ranges from −0.05°C/5 day to 0.01°C/5 day, which is much smaller than the contribution of other processes. From April 1 to May 1, the contribution of ADV was positive, indicating that the advection process played a weak heating role during the warm pool development phase. After May 1, ADV started to become negative and played an increasingly important cooling role in the warm pool. Due to heavy rainfall and river runoff over evaporation, the salinity of the seawater in the Bay of Bengal was exceptionally low. During November and December, in the western Bay of Bengal, the East India Coast Current (EICC), which flows equatorward off the east coast of India, flows around Sri Lanka and continues as a poleward-flowing West India Coastal Current off the west coast of India (Shetye et al., 1996). The EICC carries a large amount of low-salt horizontal current from the Bay of Bengal into the AS. This coastal current system is further strengthened between December and February by the westward North Equatorial Current (NEC). These low-saline waters create a near-surface halocline, which enhances stratification. Then the stratification prevents the vertical redistribution of the turbulent and radiative heat fluxes, amplifying the change in SST (Rao and Sivakumar, 1999). These low saline waters are confined within the Arabian Sea by anticyclonic eddies, which persist until April and May, promoting the formation of a barrier layer and thus favoring the development and maintenance of the ASWP.

https://doi.org/10.5194/egusphere-2023-918
Preprint. Discussion started: 8 May 2023

4 Interannual variability of the ASWP

4.1 Characteristics of the interannual variability of ASWP

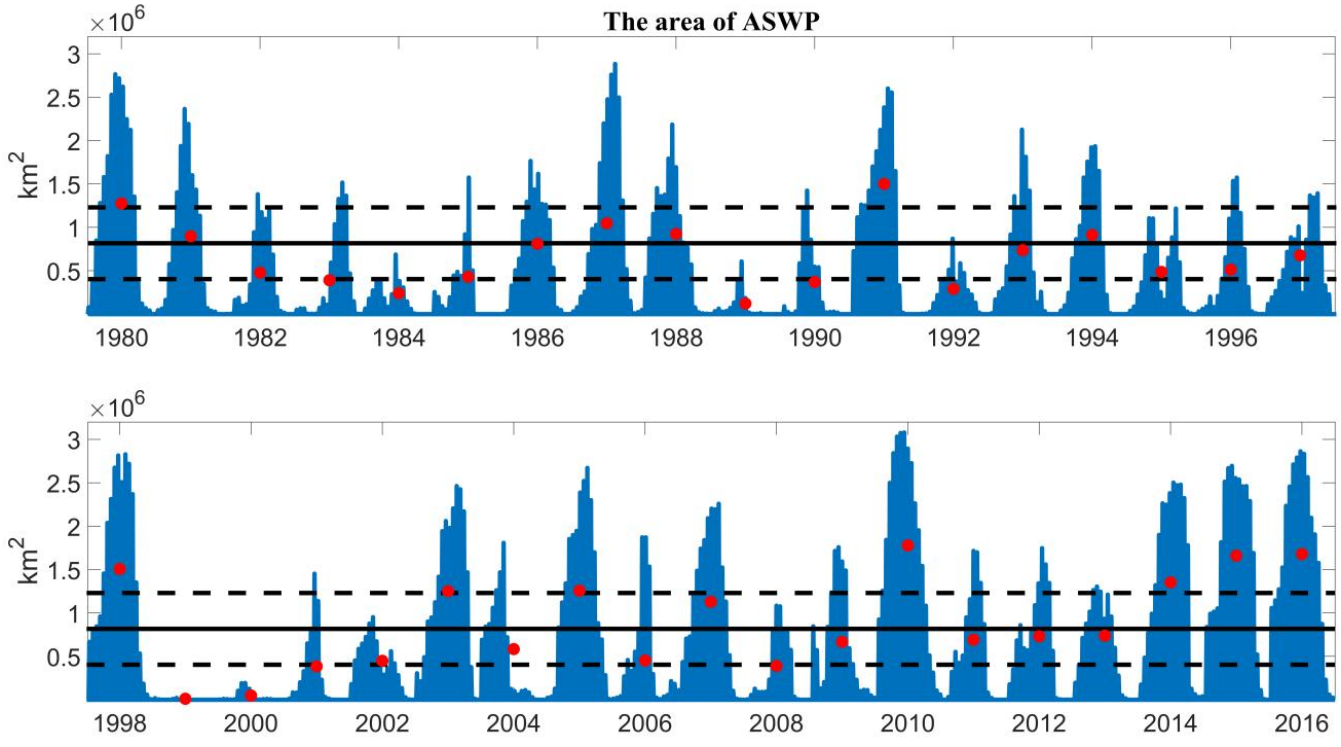

Figure 9: Time series of ASWP area from April to June 1980–2016 (red dots indicate the average area of ASWP per year). The horizontal black continuous line represents the seasonal mean, and dashed lines represent ±0.5 standard deviations.

The ASWP does not occur every year. Its intensity and extent vary from year to year. As shown in Figure 9, there has been a significant interannual variation in the area of the ASWP. The ASWP was a large area in 1980, 1991, 1998, 2003, 2005, 2010, 2014, 2015, and 2016, exceeding 0.5 standard deviations of the area and reaching a maximum of 3.1*106 km^2. In other years, the area of the warm pool has been almost negligible (1984, 1989, 1992, 1999, 2000, 2008), indicating that the ASWP is weak at this time. The weakness was related to the overall low SST in the Indian Ocean in those years.

https://doi.org/10.5194/egusphere-2023-918
Preprint. Discussion started: 8 May 2023

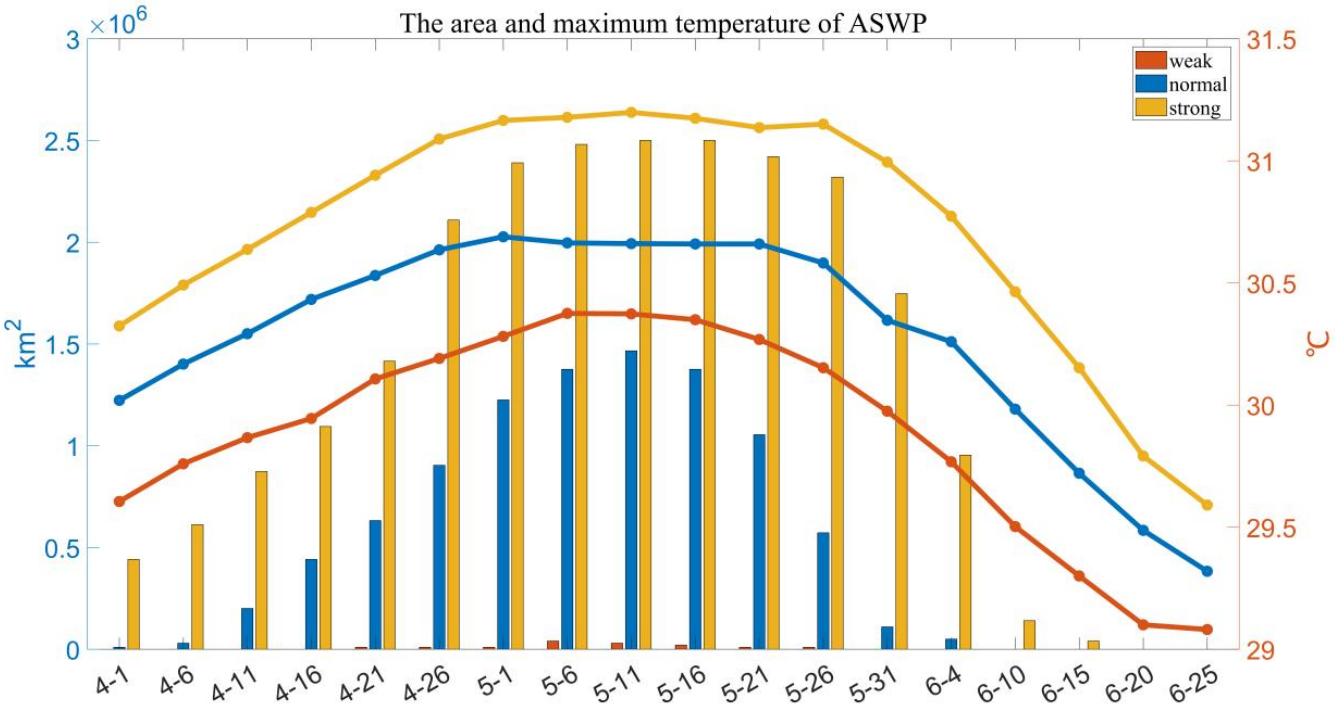

Figure 10: Variation of the area and maximum temperature of different types of ASWP from 1980 to 2016, where the bars represent the area of the warm pool (km^2), the dashes represent the maximum temperature of the warm pool (°C), red represents weak ASWP, blue represents normal ASWP, and yellow represents strong ASWP.

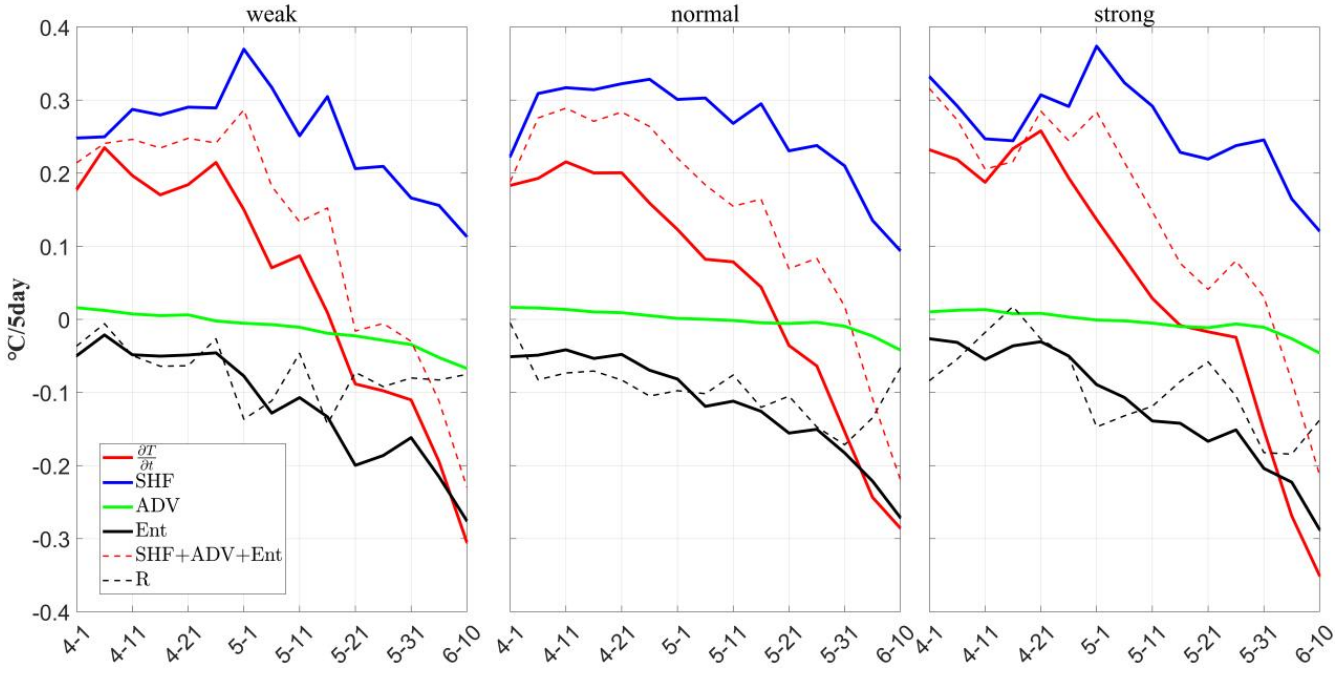

https://doi.org/10.5194/egusphere-2023-918
Preprint. Discussion started: 8 May 2023

Figure 11: ASWP mixed layer heat budget diagnosis, with weak ASWP years on the left, normal ASWP years in the middle, and strong ASWP years on the right.

Table 1. Contribution of each term to SST variation.

	SHF(%)			ENT(%)			ADV(%)		
	Weak	Normal	Strong	Weak	Normal	Strong	Weak	Normal	Strong
Heating phase	80.20	78.51	81.52	19.74	19.7	17.04	0.06	1.71	1.44
Cooling phase	31.87	35.27	38.35	53.59	54.20	52.15	14.55	10.52	9.50

Based on a half standard deviation, we estimated the average area of the ASWP for each year and identified the weak, normal, and strong ASWP years. As shown in Figure 10, the warm pool area and maximum temperature were always the highest in strong ASWP years, with an average area of $1.3*10^6$ km^2 and an average maximum temperature of 30.7°C. In normal years, the average area was $0.53*10^6$ km^2, and the average maximum temperature was 30.3°C. In weak ASWP years, the average area was only $7.8*10^3$ km^2, and the average maximum temperature was only 29.9°C. The diagnostic results of its mixed layer synthesized separately indicated similarity to the diagnostic results of climate state averaging (Figure 3,11, Table 1). During the warming phase, the temperature changes were faster in strong ASWP years (>0.2°C/5day), while the temperature changes were smaller in weak ASWP years (<0.2°C/5day). This is consistent with the faster expansion and larger area of ASWP in strong years. In strong years, the sea air flux dominated absolutely, and the quantitative values of strong, weak, and normal gradually became smaller, corresponding to the change in temperature. During the cooling phase, the cooling effect of the vertical entrainment strengthened and controlled the temperature variation of ASWP jointly with the surface heat flux. As its joint influence weakened, the advection cooling process strengthened and the warm pool weakened.

https://doi.org/10.5194/egusphere-2023-918
Preprint. Discussion started: 8 May 2023

4.2 The relationship between ASWP and IOD, ENSO

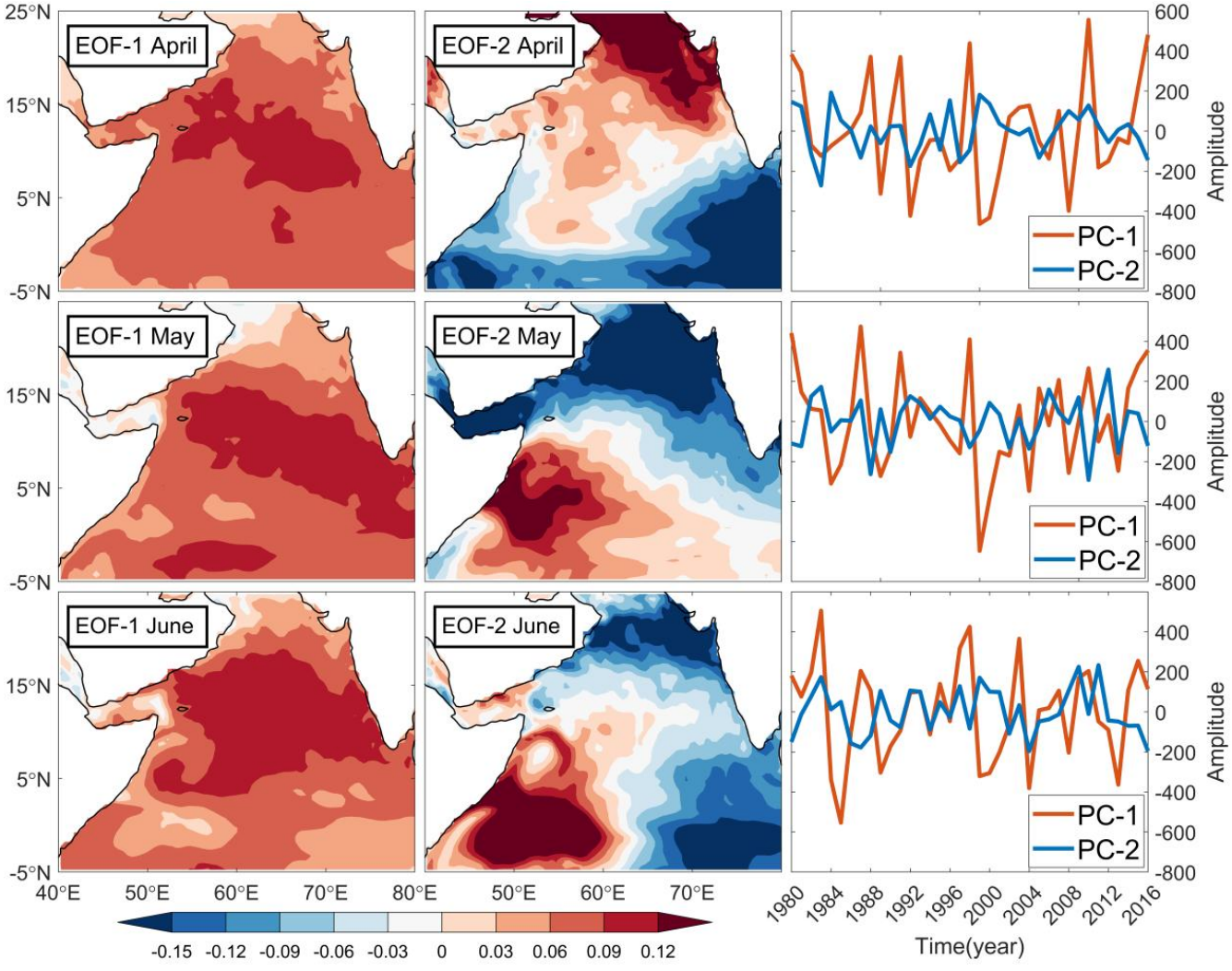

305

Figure 12: EOF1 (the first column), EOF2 (the second column), and PC1 and PC2 (the third column) of SST anomalies in the Arabian Sea for April–June.

https://doi.org/10.5194/egusphere-2023-918
Preprint. Discussion started: 8 May 2023

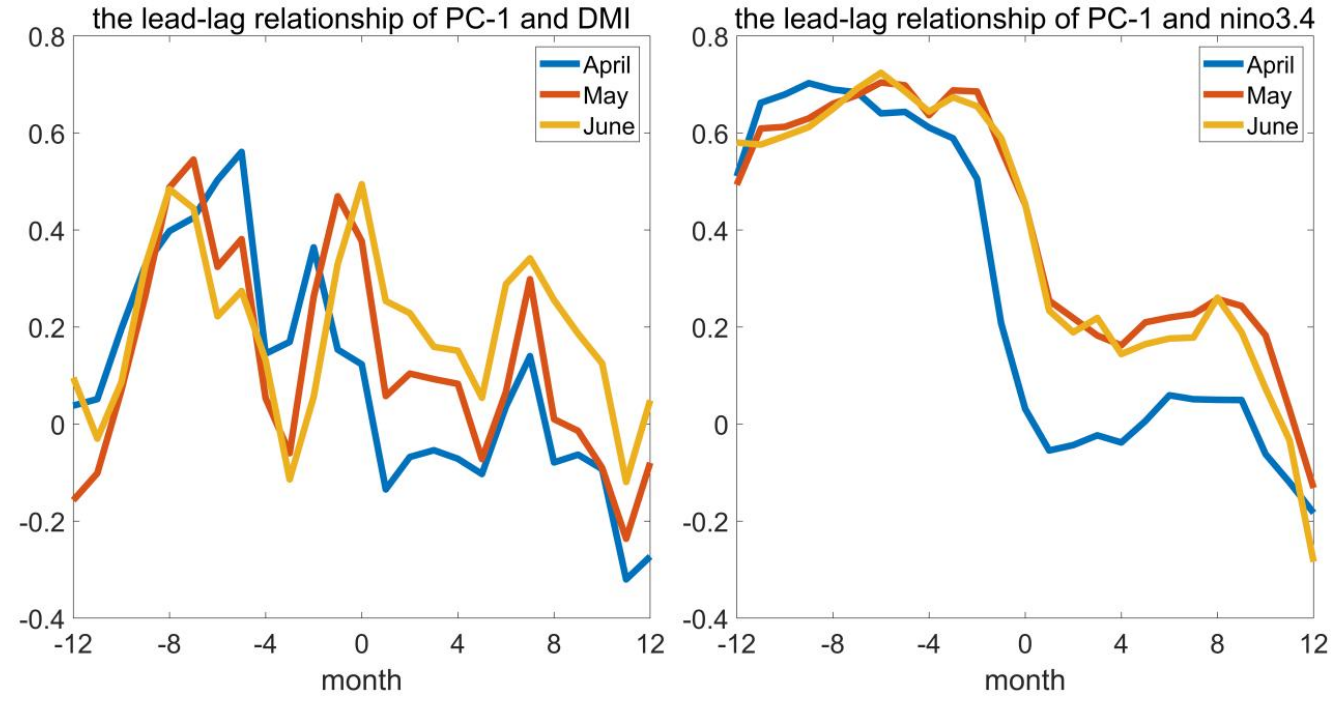

Figure 13: Lead lag correlation between PC1 and the IOD index DMI (left) and ENSO index niño3.4 (right) in April, May, and June.

The EOF analysis was conducted separately for temperatures in the Arabian Sea from April to June, and the first two modes were used for the analysis (Figure 12). The first mode variance contribution for April, May, and June was all greater than 50%. The spatial and temporal distributions were similar for the entire Arabian Sea temperature consistent variability, which was mainly related to the dominant mode in the Indian Ocean, IOB consistent mode. The Principal Component (PC) time series in April and May showed large positive peaks in 1987, 1991, 1998, 2010, and 2016, indicating that the temperature in April and May in the Arabian Sea was anomalously warm in these five years. This corresponds to several years with large ASWP areas, indicating that the large ASWP ranges in these five years were mostly due to the consistent warming of the IOB. Similarly, the years with negative peaks in the PC time series (1989, 1992, 1999, 2000, and 2008) coincide with the years with smaller ASWP areas, suggesting that these five years with smaller ASWP ranges were controlled by the IOB. The variance contribution of the second mode was smaller (about 10%) than the first. The spatial distribution pattern varied by month, but all showed inverse phase changes as well as at least two extreme centers. The PC2 also varied, and the overall amplitude of the change was smaller than the PC1.

The ASWP is part of the Indian Ocean. The most dominant interannual climate modes in the TIO are the IOB mode and the IOD mode (Schott et al., 2009). Therefore, we further investigated the effects of IOB and IOD on the interannual variability of the ASWP. The IOB is the first mode of the Indian Ocean and characterized as a consistent warming or cooling at the Indian Ocean basin scale (Xie et al., 2009). Therefore, when the IOB is in a positive phase, there is consistent warming

https://doi.org/10.5194/egusphere-2023-918
Preprint. Discussion started: 8 May 2023

across the Arabian Sea with a large range and intensity in the ASWP. These conditions occurred in 1987, 1991, 1998, 2005, 2010, 2014, 2015, and 2016. The IOD is an inherent interannual climate mode in the TIO. A dipole structure characterized the SST anomaly during positive IOD: warmer than usual SSTs occurred over large parts of the western basin, while SSTs off Sumatra were cooler than usual (Saji et al., 1999). The Arabian Sea is located in the western side of the Indian Ocean, which is part of the western IOD. Its local sea–air interaction and its interannual variation are closely related to the IOD. The left panel of Figure 13 shows that the PC-1 of ASWP was positively correlated with the IOD most of the time. The correlation coefficient reached 0.57, indicating that the ASWP had a good correlation and synchronization with the IOD.

The Indian Ocean is directly and indirectly influenced by global or other regional climate patterns, such as the ENSO. Therefore, we also considered the impact of the ENSO on the interannual variability of the ASWP. Previous research has indicated that the ENSO has an impact on SST over the Indian Ocean (Harrison and Larkin, 1998; Klein et al., 1999). Both observations and model studies indicate that the Indian Ocean warms (cools) throughout the ocean basin in March–May following an El Niño (La Niña) year (Xie et al., 2002; Lau and Nath, 2003; Song et al., 2007; Dommenget and Jansen, 2009). Kim et al. (2012) investigated the warm pool features in the Indian and Pacific Ocean and discovered that the seasonal variations in the Indian Ocean was greater than in the Pacific, which was due mostly to ENSO. The intensity of the warm pool was associated to a 5–6 months delay after the ENSO. The right panel of Figure 13 shows the lead lag correlation between the PC1 of ASWP and niño3.4. It can be seen that the ASWP was most correlated with a lag of 5–7 months in the niño3.4 index, indicating that it was modulated by the ENSO. In other words, after the El Niño (La Niña) peaks in winter, the ASWP before the summer monsoon in the upcoming year was more (less) pronounced, which is consistent with the strength of the IOWP peaking about five months after the ENSO peaked. This delay is due to the fact that the ENSO-induced teleconnection between oceans takes some time to develop.

https://doi.org/10.5194/egusphere-2023-918
Preprint. Discussion started: 8 May 2023

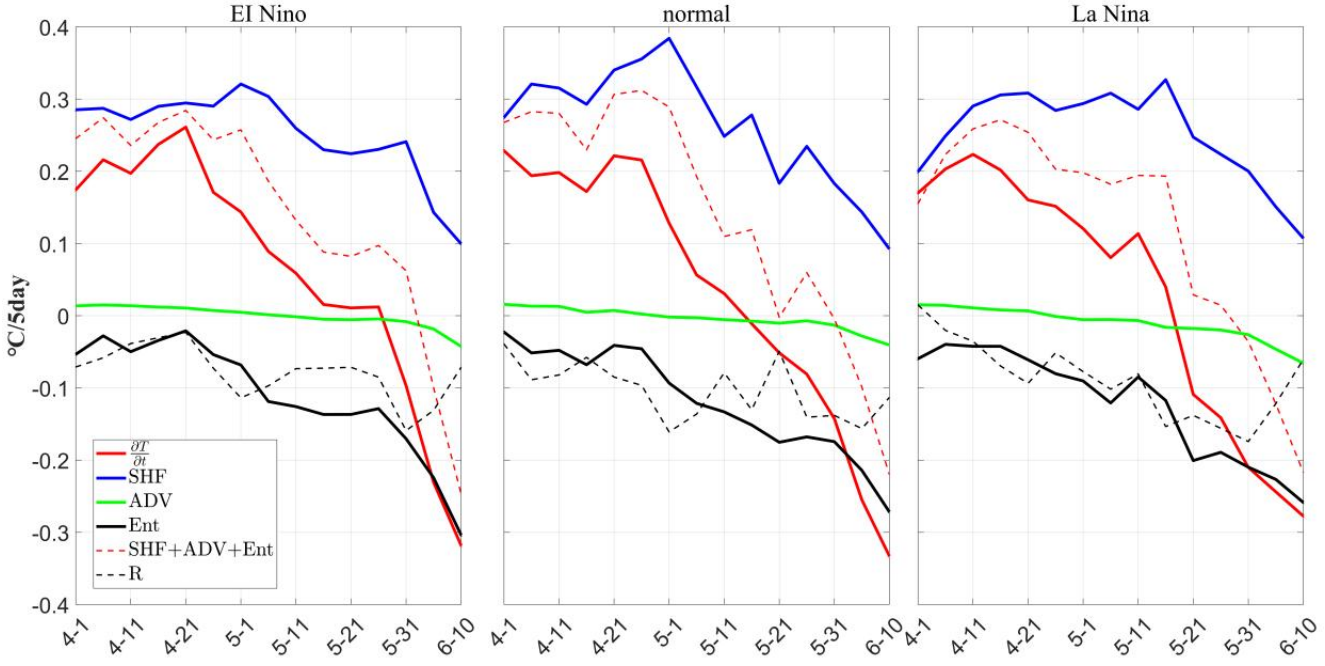

Figure 14: ASWP mixed layer heat budget with El Niño year on the left, normal year in the middle, and La Niña year on the right.

Can changes in the ENSO affect the role of different processes in the evolution of the ASWP? To explore this question, we divided the ASWP into El Niño, La Niña, and normal years, and diagnosed them separately. The results are shown in Figure 14. It can be seen from the overall trend that the change in the ENSO did not change the dominance of SHF and ENT in the evolution of ASWP. However, the surface heat flux still dominated in the warming phase, and the surface heat flux and the vertical entrainment together dominated the temperature change of ASWP in the cooling phase. It is noteworthy that although the SST warmed up during El Niño, the effect of surface heat flux did not increase significantly. However, the effect of vertical entrainment was enhanced, which may be related to the enhanced convective activity and mixing effect during El Niño.

5 Summary and Discussion

In this study, we analyzed the Intraseasonal and interannual variability of the ASWP, explored the causes of the Intraseasonal variability in the ASWP using heat budget analysis, and explored the relationship between the interannual variability of ASWP and large-scale modes using lead lag correlation. By analyzing the climatological mean sea surface temperature from 1980 to 2016, we showed that the formation and extinction of the ASWP were completed in April, May, and June. Its formation and decay rates showed asymmetry, with a decay rate twice as fast as the development rate.

The diagnostic analysis of the mixed layer heat budget using the SODA reanalysis data found that the surface heat flux had the largest effect on the ASWP mixed layer temperature. The next most important factor was the vertical entrainment, and

https://doi.org/10.5194/egusphere-2023-918
Preprint. Discussion started: 8 May 2023

the horizontal advection had the smallest effect, which is consistent with previous results. The effect of SHF on the warm pool temperature was divided into two parts, $SHF_{Q_{net}}$ and $SHF_{Q_{loss}}$. $SHF_{Q_{net}}$ was related to SWR, which is at a maximum in April due to a lack of clouds and gradually decreases with the onset of the summer monsoon and an increase in cloudiness. $SHF_{Q_{loss}}$ was related to the depth of the mixed layer and increases with the onset of the summer monsoon. During the warm pool development phase, the mixed layer was shallow and SWR is able to penetrate the mixed layer, resulting in an increase in $SHF_{Q_{loss}}$ to heat subsurface seawater. During the decay phase, the mixed layer became deeper, which greatly inhibited the penetration of SWR into the mixed layer. The ENT always played a cooling role. The increasing cooling effect made the ASWP decay rapidly. The cooling effect due to local changes in the mixed layer was the strongest.

ASWP, as part of the Indian Ocean, has had strong interannual variability. In 1987, 1991, 1998, 2005, 2010, 2014, 2015, and 2016, the area of the ASWP was large, up to $3.1*10^6$ km^2. In other years, the warm pool area was almost negligible. The average area of the ASWP was used as an indicator to classify strong and weak years. The diagnostic analysis revealed that during the warming phase, temperature changes were faster and surface heat fluxes acted more strongly in strong ASWP years. Temperature changes were smaller in weak ASWP years, corresponding to the faster expansion and larger area of the ASWP in strong years. Considering the effects of IOB and IOD on the interannual variability of ASWP, we found that the Arabian Sea, as part of the IOD, had a positive correlation between its PC1 and IOD most of the time, with a good correlation synchronization. With respect to the ENSO, the ASWP had the largest correlation at a lag of 5–7 months for the niño3.4 index, showing that it was modulated by the ENSO. In other words, the ASWP was stronger (weaker) during the summer monsoon after El Niño (La Niña) peaks in winter, which is consistent with the strength of the IOWP peaking about five months after the ENSO peaked.

However, there are many interacting factors affecting the SST variability in the Arabian Sea. In this paper, we investigated the effects of only three processes: surface heat flux, horizontal advection, and vertical entrainment. We ignored other influencing factors such as horizontal and vertical diffusion, which require further optimization of their diagnostic formulae and more comprehensive diagnostic methods. In addition, the variation of ASWP is influenced by various global scale modes. Its development, extinction, and interannual variation should be regarded as a coupled ocean–land–air process to more comprehensively and accurately grasp its variation characteristics, dynamic mechanism, and influence on various sea–air interaction processes.

Data availability. The SODA and JRA-55 dataset described in this paper is available to download at the following address: https://dsrs.atmos.umd.edu/DATA/soda3.7.2/ORIGINAL/ocean/; https://rda.ucar.edu/datasets/ds628.0/dataaccess/.

Author contributions. SWZ, XMZ and XDW designed the study. NL conducted and made the analysis. All authors contributed to the discussion of the analysis and the final manuscript.

Competing interests. The authors declare that they have no conflict of interest.

https://doi.org/10.5194/egusphere-2023-918
Preprint. Discussion started: 8 May 2023

Disclaimer. Publisher's note: Copernicus Publications remains neutral with regard to jurisdictional claims in published maps and institutional affiliations.

Acknowledgments. We thank Hui Wang and Xidong Wang for helpful discussions.

Financial support. This research was supported by the NSFC (42206029), and Southern Marine and Engineering Guangdong Laboratory (Zhuhai) (SML2020SP008).

References

Annamalai, H., Murtugudde, R., Potemra, J., Xie, S. p., Liu, P., and Wang, B.: Coupled dynamics over the Indian Ocean: spring initiation of the Zonal Mode, Deep-Sea Res., Part II., 50, 2305-2330, https://doi.org/10.1016/S0967-0645(03)00058-4, 2003.

Bauer, S. H., Gary & Olson, Donald: Influence of monsoonally-forced Ekman dynamics upon surface layer depth and plankton biomass distribution in the Arabian Sea, Deep Sea Research Papers. 38. 531–553. 510.1016/0198-0149(1091)90062-K, https://doi.org/10.1016/0198-0149(91)90062-K, 1991.

Behera, S. K., Luo, J. J., Masson, S., Rao, S. A., Sakuma, H., and Yamagata, T.: A CGCM Study on the Interaction between IOD and ENSO, J. Clim., 19, 1688-1705, https://doi.org/10.1175/JCLI3797.1, 2006.

Bruce, J. G., Johnson, D. R., and Kindle, J. C.: Evidence for eddy formation in the eastern Arabian Sea during the northeast monsoon, J. Geophys. Res.: Oceans., 99, 7651-7664, https://doi.org/10.1029/94JC00035, 1994.

Chowdary, J. S. and Gnanaseelan, C.: Basin-wide warming of the Indian Ocean during El Niño and Indian Ocean dipole years, Int J Climatol., 27, 1421-1438, https://doi.org/10.1002/joc.1482, 2007.

Dommenget, D. and Jansen, M.: Predictions of Indian Ocean SST Indices with a Simple Statistical Model: A Null Hypothesis, J. Clim., 22, 4930-4938, https://doi.org/10.1175/2009JCLI2846.1, 2009.

Giese, J. A. C. a. B. S.: SODA: A Reanalysis of Ocean Climate, Journal of Geophysical Research-Oceans, 2005.

Harrison, D. E. and Larkin, N. K.: El Niño-Southern Oscillation sea surface temperature and wind anomalies, 1946–1993, Rev. Geophys., 36, 353-399, https://doi.org/10.1029/98RG00715, 1998.

Joseph, P. V.: Warm pool in the Indian Ocean and monsoon onset, Tropical Ocean-Atmos. News Let., 53,l-55, 1990.

Kim, S. T., Yu, J. Y., and Lu, M.-M.: The distinct behaviors of Pacific and Indian Ocean warm pool properties on seasonal and interannual time scales, J. Geophys. Res., 117, https://doi.org/10.1029/2011JD016557, 2012.

Klein, S. A., Soden, B. J., and Lau, N.-C.: Remote Sea Surface Temperature Variations during ENSO: Evidence for a Tropical Atmospheric Bridge, J. Clim., 12, 917-932, https://doi.org/10.1175/1520-0442(1999)012<0917:RSSTVD>2.0.CO;2, 1999.

Krishnamurti, T. N., Oosterhof, D. K., and Mehta, A. V.: Air–Sea Interaction on the Time Scale of 30 to 50 Days, J. Atmos. Sci., 45, 1304-1322, https://doi.org/10.1175/1520-0469(1988)045<1304:AIOTTS>2.0.CO;2, 1988.

Kumar, P. V. H., Joshi, M., Sanilkumar, K. V., Rao, A. D., Anand, P., Kumar, K. M. A., and Rao, C. V. K. P.: Growth and decay of the Arabian Sea mini warm pool during May 2000: Observations and simulations, 528-540, https://doi.org/10.1016/j.dsr.2008.12.004,

Kurian, J. and Vinayachandran, P. N.: Mechanisms of formation of the Arabian Sea mini warm pool in a high-resolution Ocean General Circulation Model, J. Geophys. Res.: Oceans., 112, https://doi.org/10.1029/2006JC003631, 2007.

Lau, K.-M. and Chan, P. H.: Intraseasonal and Interannual Variations of Tropical Convection: A Possible Link between the 40–50 Day Oscillation and ENSO?, J. Atmos. Sci., 45, 506-521, https://doi.org/10.1175/1520-0469(1988)045<0506:IAIVOT>2.0.CO;2, 1988.

Lau, N.-C. and Nath, M. J.: Impact of ENSO on the Variability of the Asian–Australian Monsoons as Simulated in GCM Experiments, J. Clim., 13, 4287-4309, https://doi.org/10.1175/1520-0442(2000)013<4287:IOEOTV>2.0.CO;2, 2000.

https://doi.org/10.5194/egusphere-2023-918
Preprint. Discussion started: 8 May 2023

Lau, N.-C. and Nath, M. J.: Atmosphere–Ocean Variations in the Indo-Pacific Sector during ENSO Episodes, J. Clim., 16, 3-20, https://doi.org/10.1175/1520-0442(2003)016<0003:AOVITI>2.0.CO;2, 2003.
Li, Y., Han, W., Wang, W., and Ravichandran, M.: Intraseasonal Variability of SST and Precipitation in the Arabian Sea during the Indian Summer Monsoon: Impact of Ocean Mixed Layer Depth, J. Clim., 29, 7889-7910, https://doi.org/10.1175/JCLI-D-16-0238.1, 2016.
Liu Yanliang, Y. W., Li Kuiping: Mixed layer heat budget in Bay of Bengal ： Mechanism of the generation and decay of spring warm pool, Acta Oceanol. Sin., 35, 1-8, 2013.
Meyers, G., McIntosh, P., Pigot, L., and Pook, M.: The Years of El Niño, La Niña, and Interactions with the Tropical Indian Ocean, J. Clim., 20, 2872-2880, https://doi.org/10.1175/JCLI4152.1, 2007.
PANG Shanshan, W. X., LIU Hailong, SHAO Caixia: Multi-Scale Variations of Barrier Layer in the Tropical Ocean and Its Impacts on Air-Sea Interaction： A Review, Adv. Earth Sci., 36, 139-153, 10.11867/j.issn.1001-8166.2021.022, 2021.
Picaut, J., Ioualalen, M., Menkes, C. E., Delcroix, T., and Mcphaden, M. J.: Mechanism of the Zonal Displacements of the Pacific Warm Pool: Implications for ENSO, Science, 274, 1486 - 1489, DOI: 10.1126/science.274.5292.1486, 1996.
Rao, R. and Sivakumar, R.: On the possible mechanisms of the evolution of a mini-warm pool during the pre-summer monsoon season and the genesis of onset vortex in the South-Eastern Arabian Sea, Q. J. R. Meteorol. Soc., 125, https://doi.org/10.1002/qj.49712555503, 1999.
Rao, R. R., Jitendra, V., GirishKumar, M. S., Ravichandran, M., and Ramakrishna, S. S. V. S.: Interannual variability of the Arabian Sea Warm Pool: observations and governing mechanisms, Clim. Dyn., 44, 2119-2136, 10.1007/s00382-014-2243-0, 2015.
Sabu, P. and Revichandran, C.: Mixed layer processes of the Arabian Sea Warm Pool during spring intermonsoon: a study based on observational and satellite data, Int. J. Remote. Sens., 32, 5425 - 5441, https://doi.org/10.1080/01431161.2010.501350, 2011.
Saji, N. H., Goswami, B. N., Vinayachandran, P. N., and Yamagata, T.: A dipole mode in the tropical Indian Ocean, Nature, 401, 360-363, 10.1038/43854, 1999.
Sanilkumar, K. V. P., Hareesh Kumar & Joseph, Jossia & Panigrahi, Jitendra: Arabian Sea mini warm pool during May 2000, Curr. Sci., 86, http://www.jstor.org/stable/24109531., 2004.
Schott, F. A., Xie, S.-P., and McCreary Jr., J. P.: Indian Ocean circulation and climate variability, Rev. Geophys., 47, https://doi.org/10.1029/2007RG000245, 2009.
Seetaramayya, P. and Master, A.: Observed air-sea interface conditions and a monsoon depression during MONEX-79, Arch. Meteorol., Geophys. Bioklimatol., Ser. A., 33, 61-67, 10.1007/BF02265431, 1984.
Sengupta, D., Parampil, S. R., Bhat, G. S., Murty, V. S. N., Ramesh Babu, V., Sudhakar, T., Premkumar, K., and Pradhan, Y.: Warm pool thermodynamics from the Arabian Sea Monsoon Experiment (ARMEX), J. Geophys. Res.: Oceans., 113, https://doi.org/10.1029/2007JC004623, 2008.
Shankar, D. and Shetye, S. R.: On the dynamics of the Lakshadweep high and low in the southeastern Arabian Sea, J. Geophys. Res.: Oceans., 102, 12551-12562, https://doi.org/10.1029/97JC00465, 1997.
Shetye, S. R., Gouveia, A. D., Shankar, D., Shenoi, S. S. C., Vinayachandran, P. N., Sundar, D., Michael, G. S., and Nampoothiri, G.: Hydrography and circulation in the western Bay of Bengal during the northeast monsoon, J. Geophys. Res.: Oceans., 101, 14011-14025, https://doi.org/10.1029/95JC03307, 1996.
Song, Q., Vecchi, G. A., and Rosati, A. J.: Indian Ocean Variability in the GFDL Coupled Climate Model, J. Clim., 20, 2895-2916, https://doi.org/10.1175/JCLI4159.1, 2007.
Sprintall, J. and Tomczak, M.: Evidence of the barrier layer in the surface layer of the tropics, J. Geophys. Res.: Oceans., 97, 7305-7316, https://doi.org/10.1029/92JC00407, 1992.
Thompson, B., Gnanaseelan, C., and Salvekar, P. S.: Variability in the Indian Ocean circulation and salinity and its impact on SST anomalies during dipole events, J.Mar.Res, 64, 853-880, 2006.
Webster, P. J. and Lukas, R.: TOGA COARE: The Coupled Ocean–Atmosphere Response Experiment, Bull. Am. Meteorol. Soc., 73, 1377-1416, https://doi.org/10.1175/1520-0477(1992)073<1377:TCTCOR>2.0.CO;2, 1992.
Webster, P. J., Moore, A. M., Loschnigg, J., and Leben, R. R.: Coupled ocean–atmosphere dynamics in the Indian Ocean during 1997–98, Nature, 401, 356-360, 10.1038/43848, 1999.

https://doi.org/10.5194/egusphere-2023-918
Preprint. Discussion started: 8 May 2023

Xie, S.-P., Annamalai, H., Schott, F. A., and McCreary, J. P.: Structure and Mechanisms of South Indian Ocean Climate Variability, J. Clim., 15, 864-878, https://doi.org/10.1175/1520-0442(2002)015<0864:SAMOSI>2.0.CO;2, 2002.

Xie, S.-P., Hu, K., Hafner, J., Tokinaga, H., Du, Y., Huang, G., and Sampe, T.: Indian Ocean Capacitor Effect on Indo–Western Pacific Climate during the Summer following El Niño, J. Clim., 22, 730-747, https://doi.org/10.1175/2008JCLI2544.1, 2009.